Energy Technology
Generation, Conversion, Storage, Distribution
www.entechnol.de

Switching from Lithium to Sodium—an Operando Investigation of an $FePO_4$ Electrode by Mechanical Measurements and Electron Microscopy

*Manfred Janzen, Dominik Kramer, and Reiner Mönig**

Many physical and chemical properties of Na^+ are very similar to those of Li^+, and therefore, some electrode materials for lithium-ion batteries can also work with sodium ions. As the Na^+ ion is larger than Li^+, the strains in the host lattice are larger, which can cause deviations in the electrochemical reactions. Herein, mechanical stresses are compared, which are measured by the in situ substrate curvature method during (de)lithiation/(de)sodiation of an $FePO_4$ electrode. The (de)lithiation and (de)sodiation experiments are performed on the same electrode. According to the change of the lattice parameters, during electrode operation, Na_xFePO_4 particles experience a volume change that is 2.6 times larger than that of Li_xFePO_4. In the measurements, the composite electrode exhibits a change of the stress amplitude between operation with Li and Na by roughly one order of magnitude for $0 < x < 1$. Compared with Li^+, the mechanical stress evolution during extraction and insertion of Na^+ is highly asymmetric. The observed asymmetry in the electrochemical and the mechanical data may be explained by the different energies that are required to move an intermediary amorphous phase away from or toward the crystalline sodium-rich regions during the (de)sodiation of $NaFePO_4$.

1. Introduction

Ideal intercalation materials do not change the host structure when the concentration of the intercalated species changes. This is not the case for most cathode materials used in lithium ion batteries (LIBs). Here, the host structure relaxes to different states depending on the lithium content. This energy minimization leads to phase transformations during battery operation. Often, these phase transformations are fully reversible and do not strongly change the host lattice. This is the case in the so-called insertion materials. Such materials are used as cathodes for LIB but may be also suitable for sodium ion batteries (SIBs). This is possible because the ionic radii (Li: 76 pm, Na: 102 pm)[1] and redox potentials (Li: −3.02 V, Na: −2.71 V, both vs standard hydrogen electrode) are similar. However, the replacement of lithium by sodium can still be problematic as the larger sodium ion strains the host lattice more and, consequently, the electrode material may respond by forming phases that are different from the ones known for LIB.[2–5]

The study of this phase mechanism in the olivine material $LiFePO_4$ (LFP) received much attention since it was introduced in 1997.[6] For large particles, the long voltage plateau around 3.45 V versus lithium metal can be understood as a consequence of a two-phase coexistence between LFP and $FePO_4$ (FP) in accordance with the Gibbs phase rule.[6–10] Before and after the voltage plateau, the material shows single-phase behavior with solid solution regions at high lithium content and low lithium content.[11] The transition between the solid solution regions and the two-phase coexistence strongly depends on temperature and particle size.[12–15] By lowering the particle size, the region of the solid solution is enlarged at the expense of the two-phase regime. For very small particles with a size of 15–100 nm, the two-phase coexistence and the corresponding plateau in the galvanostatic voltage even do not exist during (de)lithiation.[14] When particles are large enough and a two-phase coexistence of LFP and FP is present, small particles may be transformed one by one,[8,16] whereas larger particles exhibit a movement of a phase boundary through the particles during lithium insertion/extraction.[17] In a galvanostatic experiment, this results in a continuous decrease in the volume fraction of one phase and an increase in the other.[18–20] In LFP, this is accompanied by a linear volume expansion/contraction of the composite electrode because the volume of the unit cell of LFP is about 6.7% larger than that of FP.[6,21,22]

The intercalation of sodium into an FP host lattice causes an increase in the unit cell volume by ≈17.6%.[23,24] Comparing the

M. Janzen, Dr. D. Kramer, Dr. R. Mönig
Institute for Applied Materials
Karlsruhe Institute of Technology
Hermann-von-Helmholtz-Platz 1, Eggenstein-Leopoldshafen 76344, Germany
E-mail: reiner.moenig@kit.edu

Dr. D. Kramer
Helmholtz Institute Ulm for Electrochemical Energy Storage (HIU)
Helmholtzstraße 11, Ulm 89069, Germany

The ORCID identification number(s) for the author(s) of this article can be found under https://doi.org/10.1002/ente.202000867.

DOI: 10.1002/ente.202000867

expansions for lithium and sodium intercalation, the volume expansion of the host lattice is larger by a factor of ≈2.6 for sodium. First, indications were found that the volume expansion of the crystal lattice cannot be directly transferred to the expansion of an FP composite electrode: Strains in an FP electrode are 4.75 higher for sodium (de)intercalation than for lithium.[25] Changing the insertion ion from lithium to sodium not only affects the geometrical expansion, but also leads to a different phase and the related mechanism of the transformation during redox reaction. The first determination of the phase mechanism for sodium (de)intercalation in olivine FP via X-ray diffraction (XRD) measurements was carried out by Moreau et al.[26] From the fully sodiated-state $NaFePO_4$ (NFP) down to a sodium content of $x = 0.7$ in Na_xFePO_4 (N_xFP), a solid solution region exists. Further sodium extraction leads to a two-phase mechanism between the end of the solid solution range ($N_{0.7}FP$) and a fully desodiated FP phase.[26] The appearance of the $N_{0.7}FP$ phase may be described as a consequence of the large lattice strains of the host structure, which enable the formation of this additional phase due to energy minimization. Later, XRD experiments confirmed the two-step-phase mechanism (solid solution range N_xFP ($x = 1...0.7$), then $N_{0.7}FP$–FP coexistence), and other groups determined the end of the solid solution range to be a sodium content depending on the source between $x = 0.7...0.6$ in N_xFP.[23,24,27–29] In this report, we have not determined the concentration values, and we designate the sodium-poor phase as FP and the sodium-rich phase as $Na_{2/3}FP$. In the literature, the reaction paths during desodiation and sodiation are often different. This difference is clearly apparent in the electrochemical data where two distinct regions exist during desodiation, and only one plateau is present during sodiation. According to Lu et al., this asymmetry results from the fact that during sodiation, the $N_{2/3}FP$ phase may be bypassed, and the FP phase transforms directly to the fully sodiated NFP phase.[27] Gaubicher et al. assumed from their XRD measurements that during sodiation, the formation of the two-phase region and the single-phase region proceed in parallel.[29] Other XRD data by Galceran et al. and Casas-Cabanas et al. point in the same direction and explain the asymmetry by a three-phase coexistence (NFP, $N_{0.7}FP/N_{2/3}FP$, and FP) that is only present during sodiation.[23,24,30]

Synchrotron-based XRD experiments of Xiang et al., however, show the same phase reaction path during desodiation and sodiation. The composition region of $x = 1...0.66$ corresponds to the well-known solid solution region of NFP followed by the two-phase coexistence of a sodium-rich ($N_{0.6}FP$) and a sodium-poor phase ($N_{0.08}FP$).[28] Xiang et al. identify an additional phase in the two-phase region of the $N_{2/3}FP$ and the FP phase.[28] Their synchrotron-based XRD measurements show a lack in the sum of volume fractions of the crystalline phases, and with a pair distribution function analysis, they conclude that the missing volume is occupied by an amorphous phase with characteristic atom distances that are similar to both the $N_{2/3}FP$ and the FP phase. The volumes of the unit cells of the $Na_{2/3}FP$ and the FP phases differ by ≈13%, and Xiang et al. assume that the amorphous phase forms to buffer the large lattice strains during the transformation between $N_{2/3}FP$ and FP.[28]

The aforementioned results from different sources regarding the reaction mechanisms (phases) in sodiation and desodiation of FP do not coincide, and therefore, it is debatable if and how the phase mechanism differs between desodiation and sodiation. With this study, we aim to contribute to this discussion. We show morphological and mechanical changes that arise by the replacement of lithium by sodium in the same FP-based electrode. In situ substrate curvature measurements are used to compare the mechanical response during insertion and extraction of lithium and sodium.[31] This technique is used in conjunction with XRD data to infer the reaction mechanisms in FP. Furthermore, scanning electron microscopy (SEM) observations of the same site of the same electrode in different electrochemical states (with either lithium or sodium) can provide further insights into morphological changes of the particles and the electrode composite.

2. Results

The insertion and extraction of ions into/from an electrode lead to changes in the composition. Here, x in Li_xFePO_4 (L_xFP) and N_xFP varies, which causes volume changes and mechanical stresses. In **Figure 1**, the measured laser deflection is plotted, which in good approximation depends linearly on the mechanical stress of the electrode. While the voltage is on a plateau, the mechanical stress of L_xFP increases and decreases almost linearly. This behavior seems to be characteristic for this material and can be observed over many cycles. Figure 1 shows the last three out of 11 cycles before the lithium cell was converted into a sodium cell and the first three cycles of the freshly converted cell then cycling with sodium as insertion metal.

After the conversion to sodium, the cell is installed again into the setup and shows a slightly higher tensile stress. Most of this stress difference happens during the dissolution of the lithium reference electrode, which was performed in an effort to remove all Li and Li^+ from the cell before inserting sodium, and a smaller part of the stress change is due to reinserting the cell into the same position in the stress setup (both effects are

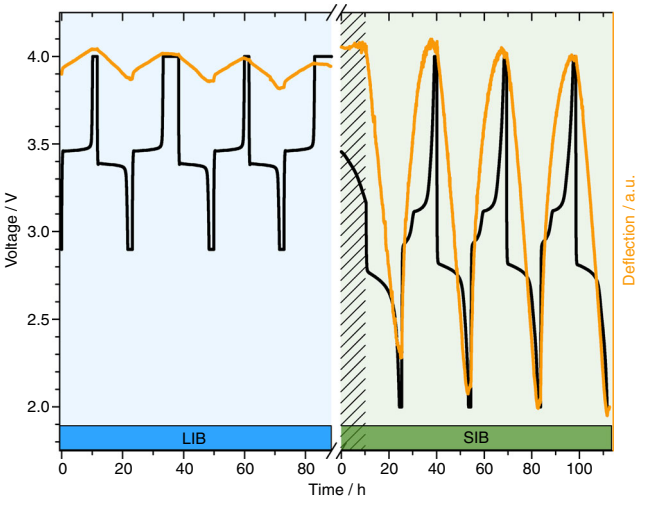

Figure 1. Galvanostatic cycling of FP: insertion/extraction of Li into/from FP (blue) and insertion/extraction of Na into/from the same electrode (green). Within the break of the horizontal axis, electrolyte and counter/reference electrodes were replaced. The hatched region corresponds to an open circuit period before Na cycling starts.

located within the break of the axis of Figure 1). After that, the converted and installed sodium cell shows a voltage decrease from 3.47 to 3.16 V during an initial open-circuit voltage (OCV) period, whereas the stress stays almost constant. Afterward, again, a consistent and repetitive electrochemical and mechanical action is recorded for the sodium cell.

Electrochemically, Figure 1 shows the expected behavior consisting of a two-phase plateau for LFP. For NFP, two features during desodiation and one sloped flat region during sodiation are expected and are clearly visible.[6,26] As sodium insertion starts, compressive stress builds up in the electrode. In comparison with lithiation, the first sodiation leads to a stress level that is higher by a factor of 10.9 (first half cycle). Upon further cycling, this stress amplitude (difference between maximum and minimum stress of a cycle) increases further. For example, the stress amplitude of the first full cycle is 12.1 times larger than that of the last lithium cycle. After the cycles shown in Figure 1, the converted cell was further tested, and in the subsequent cycles, the stress amplitude moderately increased by roughly ≈0.8% per cycle, so that it exhibited about twice the stress amplitude after 100 cycles. The substrate curvature setup yields very reproducible stress data, and this increase in stress has to be attributed to changes in the electrode. An experimental difficulty for this work was the determination of a correct factor for the ratio of the stress amplitudes between lithium and sodium. This is complicated because of technical problems with the transition from lithium to sodium. In this process, the electrode can delaminate, which makes the stress measurement by substrate curvature impossible. From five attempts, we obtained only two cases where, after the conversion, the laser beam stayed roughly at the same position (deflection) and where the electrochemical signal upon further cycling was reliable. The results of both experiments are very similar. The transition leads to an increase in the stress range between lithium and sodium of about one order of magnitude (the experiments lead to an increase in the factors of 10.2 and 10.9 for comparing the last delithiation with the first sodiation). Therefore, it seems reasonable to assume that the stress amplitude increases by one order of magnitude when lithium is replaced by sodium in the composite electrode.

In this work, deflection is reported in arbitrary units because the elastic properties of the components are not known, and a reasonable assessment requires a finite-element analysis.[32] If we assume similar mechanical properties and thicknesses of the components as was used for $Li_4Ti_5O_{12}$-based composite electrodes,[32] the stress range in the LFP composite electrode would be around 210 kPa, and consequently, the stress in the NFP electrode would be around 2.55 MPa (**Figure 2**). This is a rough estimate of the stress level of the porous composite electrode, and it should be noted that the stresses inside the particles are expected to be orders of magnitude higher (see 1 GPa according to phase field simulations).[33]

Besides the amplitude of the mechanical stress, also the dependence of the mechanical stress on the ion content is different between operation with lithium and sodium. Figure 2 shows a comparison of the stress profiles during cycling, for the last lithium cycle and the first sodium cycle of Figure 1. Both curves are scaled, so that they exhibit the same magnitude; i.e., the lithium curve is stretched by about one order of magnitude. The ion content on the horizontal axis is estimated based on the

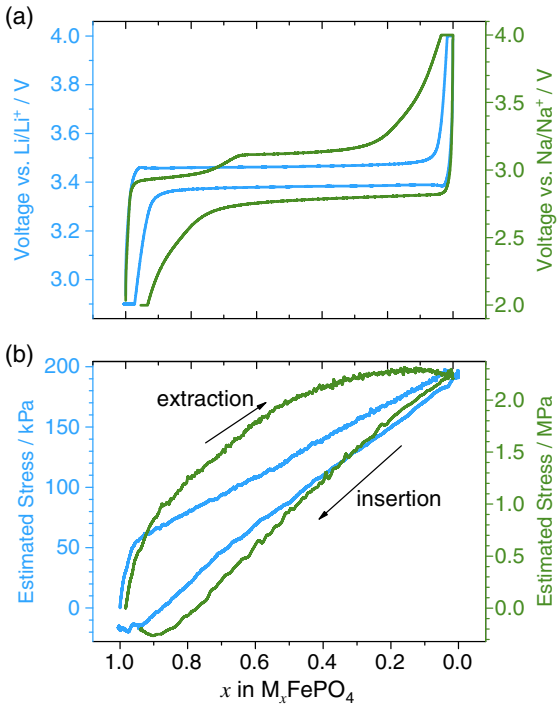

Figure 2. Comparison of a) electrochemical data and b) corresponding mechanical stress data during galvanostatic extraction and insertion of Li in the last cycle (blue, C/10) and Na in the first cycle (green, C/13) for the same FP electrode.

maximum charge capacity of the corresponding cycle. The insertion of lithium and that of sodium lead to a similar stress development where the stress evolves quite linearly with increasing ion content for LFP and NFP. During lithium extraction, LFP also shows a linear dependence on the ion concentration except at high concentrations. Sodium extraction from NFP is the only case where the stress dependence is highly nonlinear. Desodiation causes a curved stress profile where the slope of the tensile stress decreases with lower sodium content. The combination of linear sodiation and nonlinear desodiation leads to a larger hysteresis in the stress curve for NFP in Figure 2.

Figure 3 shows two consecutive galvanostatic cycles of LFP and NFP with different rates together with their mechanical stress profiles. Before each experiment, a 2 h potentiostatic hold at 2.9 and 2 V, respectively, was performed to make sure that the electrode is fully lithiated/sodiated. The ion concentration in all cycles was calculated by relating the capacities to the delithiation/desodiation capacity of the slower cycle under the assumption that full lithiation/sodiation is reached at the low rate. In (de)lithiation, both rates (C/25, Figure 3a; C/9, Figure 3b) show the two-phase plateau with the linear increase and decrease of mechanical stress in the plateau region. Besides the slightly larger hysteresis (overpotential) in the voltage curve for the C/9 cycle, the two cycles are very similar, especially in the mechanical stress response. Differences are more pronounced for sodium. In the very slow cycle with C/52 (Figure 3c), the details of the electrochemical reaction are visible in the voltage profile, and the so-called plateaus are clearly distinctive during sodiation and desodiation. The mechanical stress strongly curves

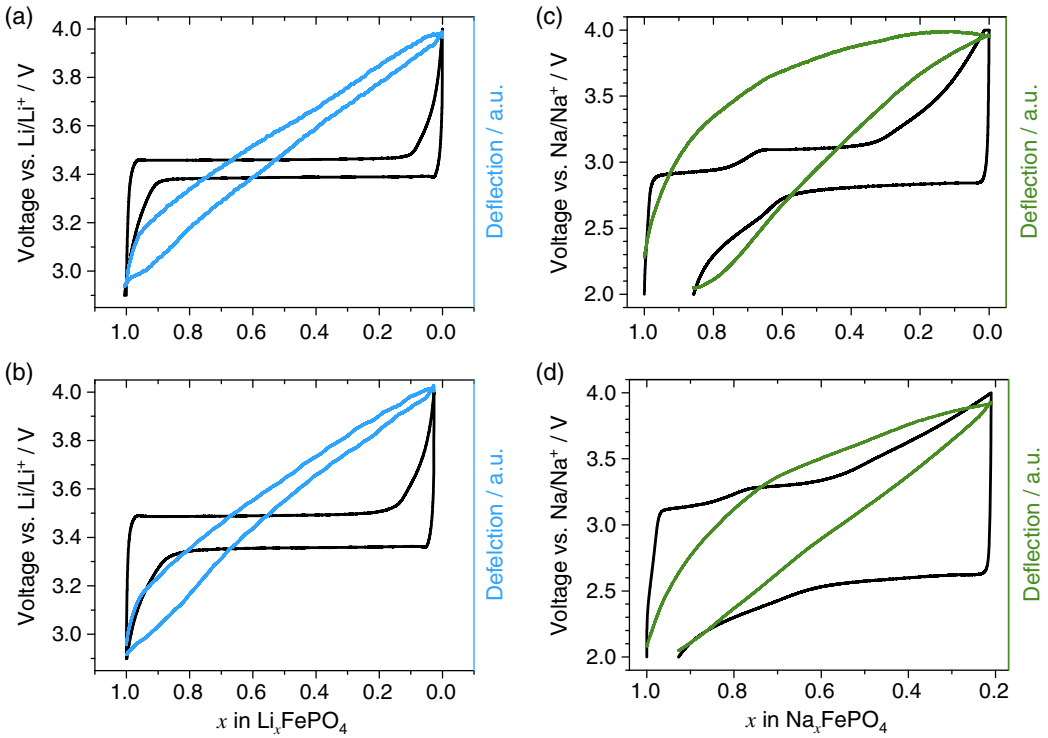

Figure 3. Voltage and mechanical stress evolution of lithium (blue) and sodium (green) extraction and insertion in M_xFePO_4 (M = Li, Na) for different rates. a) C/25. b) C/9. c) C/52. d) C/9.

at the beginning of the desodiation process and reaches saturation toward the end. Considerable differences appear if the rate is increased to C/9 (Figure 3d). During desodiation, the electrochemical curve shows less pronounced voltage steps as in the C/52 cycle and a larger hysteresis (overpotential) between desodiation and sodiation. In this fast cycle, the development of the mechanical stress in desodiation is similar to the slow cycle, except that at the end of desodiation, still a positive slope in the stress exists. The mechanical stress profile during this fast sodiation is in reasonable agreement with the one obtained for slow sodiation.

To further investigate kinetic effects in NFP, a galvanostatic measurement with C/26 was performed, and subsequently, a measurement consisting of current pulses of a duration of 60 min each followed by 30 min of open circuit periods was performed (**Figure 4**). The same current was used for the galvanostatic measurement and for the pulsed measurement. In Figure 4, the time domain of the galvanostatic measurement is stretched by a factor of 1.5 to account for the 30 min interrupts in the pulsed data. During the first 10 h, in the range of $x \approx 1...0.66$ in N_xFP, the voltage slightly increases both in the peak voltage as well in the relaxed voltage, which is the voltage at the end of the OCV periods. Once the electrode reaches the two-phase coexistence region between N_xFP and FP, the peak voltage still slightly increases over time, but the relaxed voltage reaches an almost composition independent value of 3.06 V (dashed line) between $x \approx 0.66.0.33$. Beyond $x \approx 1/3$, which is around the time when N_xFP and FP are expected to be present in similar volume fractions,[28] the relaxed voltage also starts to rise. At the beginning of the two-phase coexistence region, the

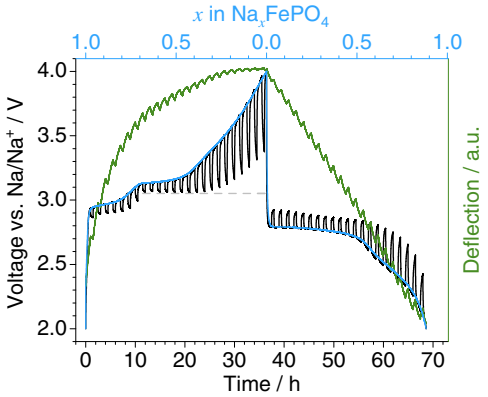

Figure 4. Relaxation behavior of FP with applied current pulses and open circuits on sodium extraction and insertion in black and a measurement with the same current without interrupts in blue.

relaxation of the cell voltage is 0.07 V and increases up to 0.60 V during the course of desodiation. The general shape of the mechanical stress profile of Figure 4 is the same as the one in Figure 2. The mechanical stress that is due to the relaxations is relatively small. During desodiation, the stress relaxes toward compression, whereas during sodiation, it relaxes toward tension. The stress relaxations become smallest when full desodiation is approached.

Also in the electrochemical data, sodiation is very different from desodiation, and Figure 4 starts with a long voltage plateau into sodiation. During this plateau, the relaxation effects are only moderate, and the relaxations of the voltage vary between 0.13

and 0.11 V. They increase toward the end of sodiation to a maximum of 0.29 V, which is still significantly lower to what is observed at the end of desodiation. The relaxation effects in the mechanical stress are relatively small at the beginning of sodiation and increase toward the end. The maximum stress changes caused by the interrupts and resumptions are similar between sodiation and desodiation.

Sodiation leads to a relatively large expansion. SEM images of the same particle recorded in the lithiated state (**Figure 5**a) and in the sodiated state (Figure 5b) directly show the volume expansion. In particular, along the length of the particle, strong changes can be seen. An SEM image analysis of 90 particles show, on average, an elongation of 4.4% in length and 1,8% in width from lithiated to sodiated. This nonuniform volume expansion causes mechanical stresses, which can lead to damage. Figure 5c shows a particle that developed cracks during sodiation (Figure 5d) then expand further during desodiation (Figure 5e). Such damage was only found in large particles. The formation of cracks was identified to happen both during sodiation as well as during desodiation.

Changes not only happen at the level of individual particles, but they are also very strong at a larger scale. Images of the

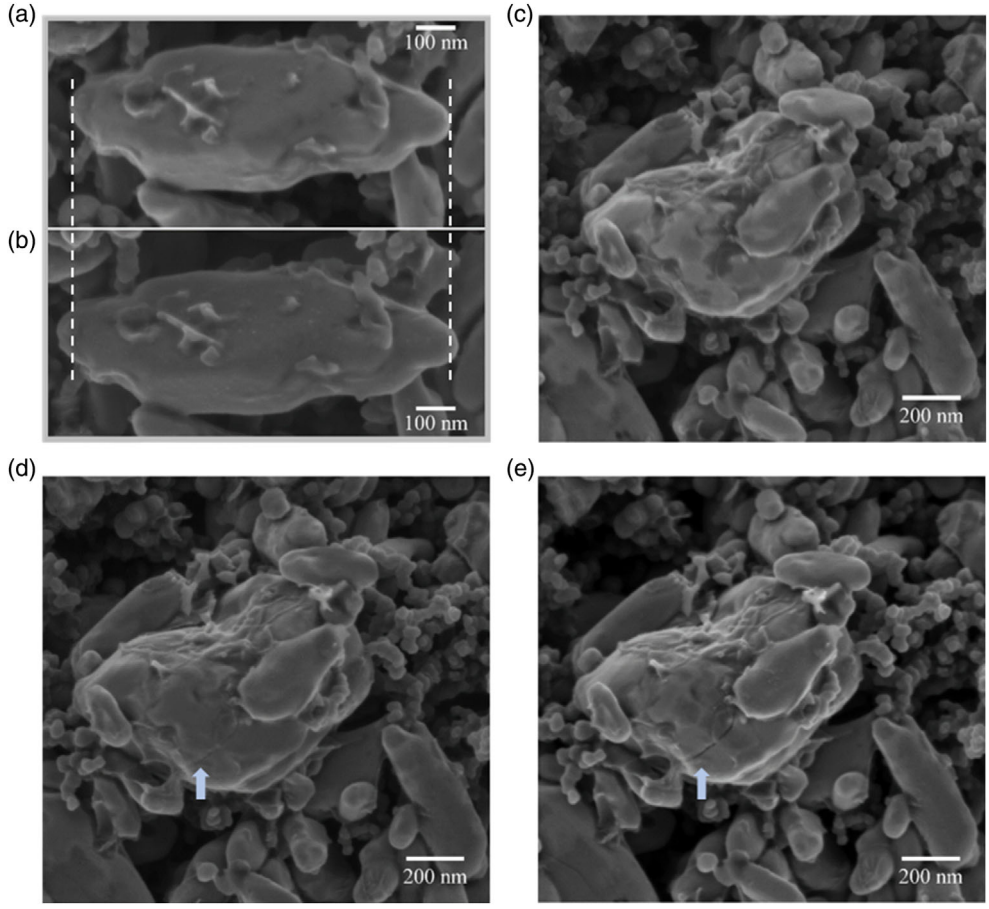

Figure 5. SEM observations of particles in different electrochemical states. a,b) Compare a single particle in the lithiated and the sodiated state. c–e) Compare a small region of the electrode from c) the delithiated state through d) the sodiated to e) the desodiated state.

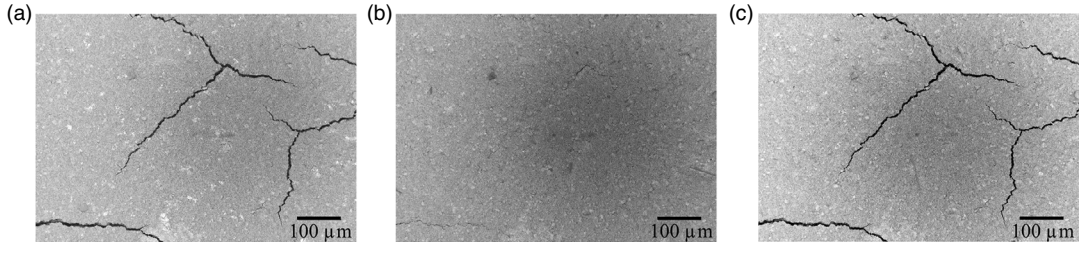

Figure 6. SEM images of the same site of the composite electrode in three different consecutive electrochemical stages: a) delithiated, b) sodiated, and c) desodiated.

composite electrodes were taken by SEM. **Figure 6** shows the same location in different states. In the delithiated state, the electrode exhibits cracks, which are a result of the electrode production process where the cracks often form during drying. In this process, the solvent *N*-methyl-2-pyrrolidone (NMP) evaporates, and the slurry shrinks and solidifies. If this happens too fast, cracks such as the ones in Figure 6a are the consequence. Delithiation of the electrode does not change the electrode composite, and no changes between the lithiated and delithiated states (Figure 6a) are detected by SEM. Once sodium is inserted, large compressive stresses form in the electrode as reported in Figure 1 and lead to a deformation of the electrode as shown by comparing Figure 6a,b. In the sodiated state, the drying cracks are not visible anymore due to the action of the large compressive stress. During extraction of sodium, the cracks then appear again (Figure 6c).

3. Discussion

3.1. Volume Expansion of Particles and at the Electrode Level and Consequences

In the SEM observations, no detectable changes are found between the lithiated and delithiated states, but clear changes occur between the sodiated and desodiated states. These changes consist in the expansion of individual electrode particles but, surprisingly, also in the larger scale motion in the composite electrode. These strong changes of the composite electrode are most likely the consequences of the expansion of the crystal lattices of the electrode particles due to ion insertion and extraction. The expansions that were observed for sodium at the level of individual particles (Figure 5) seem to be below or at the level to what is expected from the XRD data in the literature. The measured increase in the particle dimensions (4.4% in length, 1.8% in width, mean values for 90 particles) is comparable to the increase in the crystal structure parameters ($a = 1.3\%$, $b = 3.4\%$, $c = 5.2\%$) from LFP to NFP.[26] Also, the anisotropy of the expansion seems to be present in the SEM images of individual particles, suggesting that at least some of the particles are single crystals. The LFP/NFP particles here do not show the often observed facets that are indicative for single crystallinity.

The larger mechanical stresses of NFP lead to accelerated degradation. In some experiments, up to 100 cycles were performed with a total loss in a capacity of ≈30%, and mechanical degradation was found already after the first cycle when inspecting particles (Figure 5). Damage was only found in the larger particles. A particle size dependence is not uncommon for the fracture of electrode particles, and several explanations exist why damage is preferred in larger particles.[34] In the case here, the large particles where the cracks were found were not facetted and, therefore, may not be single crystals. It is plausible that the cracks form due to the anisotropic expansion of the crystallites within the polycrystalline particles.[35] If particles consist of crystallites/grains, the orientation of the grains may matter for the generation of stress. Mechanical damage most likely happens then at grain boundaries where neighboring grains expand in different directions.

Mechanical effects are not only present in individual particles, but also on the larger scale cracks open and close (Figure 6), and the electrode moves macroscopically. Such long range effects are not foreseeable just by comparing the expansion of the crystallites for lithium and sodium insertion. These morphological changes at the electrode level correlate with relatively strong mechanical stresses that were measured inside the composite electrode. The factor in the mechanical stress as determined by a laser beam deflection of 10.9 is about four times higher than what the volume change of the particles would predict. Likewise, strains of an FP composites for lithium and sodium intercalation are larger than the change of the crystal lattice volume.[25] Electrodes are made by coating a slurry onto the current collector. During drying, the final structure of the composite electrode forms. Such electrodes are porous, and besides polyvinylidene fluoride (PVDF) binder and carbon black, they consist of the active material (LFP). As PVDF and carbon black are only minor components in terms of volume, the LFP particles are mostly in direct contact. If LFP is cycled, the particles will shrink first and then expand, and only moderate stresses may arise. Once lithium is replaced by sodium and NFP is formed, the volume will expand by more than 10% versus LFP. This is the first time when the volume of the particles is larger than during electrode production. In this configuration, an increased number of particles may come into contact with each other, and the electrode morphology may change. The increased number of particle contacts would then lead to a stronger stress–strain response and higher stresses than predicted just by considering crystalline volume expansion. In general, it may also be assumed that for larger strains, tensile and compressive responses will be nonsymmetrical. Large tensile stresses can be accommodated by the pores and the binder, whereas large compressive stresses lead to increased direct contacts between particles of the active material. This effect may depend on the texture of the electrode and the shape of the particles. The binder PVDF is known to be viscous and can move away from regions of high stresses.[36] It may expected that its viscosity is even higher once it is soaked by the electrolyte solvent. In this case, ratcheting effects during cycling may be observed where the stresses even increase with increasing cycle number. The increase in the stress amplitude with cycle number as shown in Figure 1 after switching to sodium may be such a case. Our observations indicate that the composite electrode reacts nonuniformly and presumably irreversibly to compressive stress, and that an extrapolation of volume changes from the crystal structure to the electrode level is not straightforward for electrodes where the particles significantly expand after cell production.

3.2. Mechanical Stress and Voltage during Ion Insertion and Extraction

In accordance with Gibbs phase rule, the voltage plateau for the insertion and extraction of lithium in FP indicates the coexistence of two phases. The corresponding linear evolution of mechanical stress is in good agreement with a two-phase coexistence. The linear stress accumulation indicates a constant change of the electrode volume that can be attributed to a constant volume change of the electrode particles. The lithium-rich and lithium-poor phases have different unit cell volumes, which result in a volume change of a particle that undergoes a phase transition between these two phases. For a two-phase coexistence

in LFP, the particle size is a relevant factor: for a particle size of 40 nm, two coexisting phases are not expected.[14] The particle sizes in the electrodes used here are clearly larger (Figure 5); therefore, a two-phase mechanism seems plausible. Before and after the two-phase coexistence, when the voltage is not on the plateau, the phases of LFP and FP are present. These phases show a certain lithium ion solubility before the two-phase region is reached. In these single-phase regions, the voltage depends strongly on the lithium concentration of the solid solution. Even larger potential variations are expected as soon as the limits of the solubility ranges are exceeded: Lithium insertion into the LFP phase is hardly possible, and lithium extraction from the FP phase is impossible; currents in those directions result in double layer charging, which is a surface effect that—in the case of micrometer-sized particles—will hardly be visible in the stress signal. The linear evolution of the mechanical stress does not seem to be significantly affected from these single-phase regions. Small deviations from the linear behavior are noticeable at the beginning and the end of delithiation, when only the LFP phase or the FP phase is present. In these regions, the mechanical stress evolves with a different slope than in the two-phase coexistence region, and these small deviations from the linear behavior in the two-phase region may cause the small hysteresis in the mechanical stress curve. Overall, the mechanical data during delithiation and lithiation are quite similar.

By changing the insertion ion from lithium to sodium, which is chemically relatively similar to lithium, the mechanical response becomes characteristically different between desodiation and sodiation. While sodiation leads to a linear stress evolution that is similar to (de)lithiation, desodiation results in a nonlinear stress profile, where the stress starts to curve already that at high sodium content. The shape of the nonlinear mechanical stress curve appears to be quite smooth; i.e., no features are present that can be easily associated with the phase regions, which are known from XRD data. The different evolution of the mechanical stress during sodiation and desodiation gives a hint toward a directional dependence of the reaction pathway.

The reversibility of the electrochemical processes may also be characterized by considering the energy efficiency of individual processes. The electrochemical cell stores and releases energy, and power is provided in an electrical form as voltage and current. Ideally, the difference in electrical energy between charge and discharge is zero, but in practical cells, there are always overvoltages (overpotentials) that consume energy and lead to the dissipation of energy. This irreversible energy can drive different processes and eventually is lost as heat. One of the processes that is visible in the experiments presented here is mechanical deformation. Just as in mechanical testing, it can be either reversible as in the action of a spring that loads and unloads or it can be dissipative. Dissipative processes show a nonlinear stress–strain dependence, for example, as known from plasticity. In the experiments (Figure 2), the stress in the composite electrode is measured, but a strain is not recorded, and an analysis is, therefore, difficult. The fact that the phases change and with them their mechanical properties are altered complicates a mechanical assessment even further. Nevertheless, a rough estimation can be made by considering that the expansion of the electrode depends linearly on the concentration of the insertion ions.[25] In this way, the energy efficiency of extraction and insertion of lithium/sodium from/into LFP and NFP can be compared. Electrically, lithium shows less of a hysteresis and exhibits an area between charge and discharge of 0.11 V and sodium an area of 0.52 V (integrated between $x = 0$ and 1). The difference of factor of 5 between both insertion ions is a consequence of the less reversible reaction pathway of NFP. Mechanically, this irreversibility is even more pronounced, and the difference in the estimated dissipated energy is much higher: For lithium, the area yields 37 kPa, and for sodium, the irreversible mechanical energy is 823 kPa (again integrated between $x = 0$ and 1). Cycling with sodium produces not only about ten times higher reversible stresses, but also leads to a ≈20 times higher dissipation of the mechanical energy in the electrode. Possible paths for energy dissipation are phase boundary motion, damage in particles as the cracks observed in Figure 5, and plastic deformation of the binder leading to the long range deformations shown in Figure 6. The small irreversible mechanical energy of LFP then correlates with the fact that no mechanical or structural damage is found in the same electrode when it is cycled with lithium.

3.3. Reaction Pathways and Rate Dependence

Desodiation starts with the solid solution region of N_xFP with $x = 1...0.66$ and ends with an ascending voltage that transitions to a kink at the start of the two-phase coexistence of $N_{2/3}$FP and FP. At the beginning, this two-phase coexistence region exhibits a plateau similar to the two-phase region of FP and LFP. Further desodiation leads to a deviation from this plateau with a rising voltage at $x \approx 0.3$ in Figure 3c (C/52). Sodium insertion and extraction are much more rate-limited than that of lithium. Figure 3d shows strong overpotentials already at a rate of C/9, and while running with lithium, the same electrode does not show significant overpotentials when the rate is changed the same way (Figure 3a,b). In the case of sodium, also about 20% of the capacity is lost, and the limiting voltage for desodiation is already achieved at $x \approx 0.2$. As usual for galvanostatic measurements, when the rate is increased, the voltage profile becomes more blurred; nevertheless, the characteristic features are still discernible. The quite horizontal plateaus develop a slope, and the deviation from the typical two-phase behavior shifts from $x \approx 0.3$ to $x \approx 0.55$. The earlier deviation from the plateau voltage is easily shown by comparing Figure 3c with 3d. Comparing the two full cycles, the location of the largest overpotential can be identified and occurs when the voltage deviates from the two-phase plateau. Whatever happens during this deviation may be the most rate limiting process of the sodium cell.

The two-phase coexistence is even more evident in relaxation experiments. Figure 4 shows that the voltage relaxes to a voltage that is composition-independent (marked by the dashed line). This figure also contains an experiment without relaxations that agrees reasonably well with the unrelaxed part of the interrupted measurement. This indicates that the overall behavior is not altered due to the interrupts. In the two-phase region, a very horizontal plateau can be found in the relaxed voltage. This plateau extends to lower concentrations than the slightly sloped plateau that is visible in the curves under current. This observation

suggests that the observed voltage deviation on the plateau at least partly originates from kinetic limitations of this material.

3.4. Possible Origin of Asymmetry of Reaction Path

A rise in voltage at the end of a two-phase plateau suggests the completion of a phase transformation and is often be attributed to a change in the concentration of the insertion ion within a single-phase region. This is, for example, the case for LFP where a steep voltage rise beyond 3.5 V is observed when FP (oxidation state of Fe^{3+}) is present everywhere in the sample (Figure 2a). For sodium, this effect seems to set in earlier (at higher concentrations) as shown by comparing the blue and green curves of Figure 2a. It seems plausible to associate the observed deviation from the plateau with the end of the two-phase reaction and the appearance of Fe^{3+}. The voltage of the cell results from the regions of the electrodes close to the electrolyte. If the FP (Fe^{3+}) forms at the perimeter of the particles and covers the whole interface to the electrolyte, the voltage of the cell can rise beyond the plateau voltage. For NFP, this happens far before the electrode is completely desodiated, and a full desodiation of the perimeter of the particles would only be possible as long as the sodium transport from the inner part to the outer part of the particles is suppressed.

The fact that there is a large lattice mismatch between $N_{2/3}FP$ and FP suggests that the motion of the phase boundary is mechanically very difficult and probably requires high driving forces. Such driving forces can only be achieved by large gradients of sodium within the FP phase at the outer part of the two-phase particles. Once the concentration reaches zero at the perimeter in all particles, the voltage will rise beyond the plateau voltage, although the end of the phase transformation has not yet been reached. Sodiation is not symmetrical to desodiation. During sodiation, the perimeter of the particles will consist of $N_{2/3}FP$, and to establish a concentration gradient, it needs to contain higher levels of sodium at the perimeter of the particle. This is a completely different situation from desodiation and probably does not lead to a kinetic limitation. These arguments may explain the asymmetric behavior of the cell in terms of voltage and the even more pronounced asymmetry in the mechanical stress. The high stresses that appear during desodiation may be a consequence of the large concentration gradients, which also cause large gradients in stress and high stresses around the perimeter of the particles.

Xiang et al. report the existence of an amorphous buffer phase between $N_{2/3}FP$ and FP that is supposed to accommodate the high mismatch in lattice strains. One can imagine that during sodiation, the transformation of the amorphous phase to the newly formed crystalline $N_{2/3}FP$ phase might result in the thermodynamically more stable orthorhombic maricite[37] instead of the metastable $N_{2/3}FP$, which has the olivine structure of triphylite LFP. As the maricite structure has no free channels for Na^+ diffusion, poor electrochemical performance is assumed.[38,39] The good cycle stability observed indicates such a maricite formation does not take place. This is in agreement with Ostwald's empirical step rule that suggests that the less stable polymorph crystallizes first.[40–42] It is also in agreement with the Ostwald–Volmer rule stating that the phase with the lower density forms first[43] (olivine NFP: ≈3.61 g cm^{-3}, maricite NFP ≈ 3.71 g cm^{-3}, with parameters from the previous studies[26,44]). According to the observed stable cycle performance, the olivine phase of NFP seems to be stable enough to not undergo a solid-state transformation to the thermodynamically favorable maricite structure.

The observed amorphous phase may not only mitigate the lattice mismatch, but also influence the dynamic interaction of the phases $N_{2/3}FP$ and FP. To grow one phase at the expense of the other, the amorphous phase needs to move. During desodiation, the amorphous phase consumes $N_{2/3}FP$, whereas during sodiation, it consumes FP, as shown in **Figure 7**. This requires amorphization at its left boundary and crystallization at the right boundary (Figure 7). It seems obvious that this is not a symmetrical process, because different phases amorphize and crystallize during (de)sodiation. It is quite likely that $N_{2/3}FP$ and FP behave very differently during these processes.

Even in the case that amorphization and crystallization of $N_{2/3}FP$ and FP are similar, there are very basic mechanical reasons for a reaction asymmetry. Solid-state amorphization

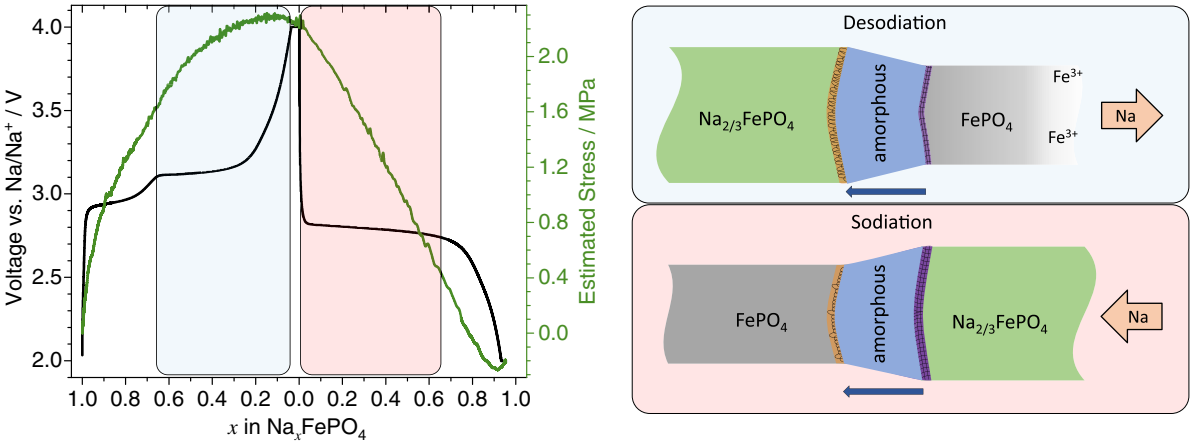

Figure 7. Schematic of the mechanism inside the particles during the two-phase coexistence of FP (gray) and $Na_{2/3}FePO_4$ (green) and the corresponding regions of the voltage and mechanical curve. The amorphous phase (blue) moves through the particle upon sodiation and desodiation. This motion consists in the amorphization (orange) of one phase on the left and the crystallization (violet) of the other phase on the right-hand side.

requires defects such as dislocations and vacancies, and the concentration of vacancies depends on the mechanical stress.[45–48] In thermodynamic equilibrium, the concentration of vacancies is lower in compression than in tension, and therefore, it can be expected that amorphization is impeded in compression compared with tension.[49] As the unit cell volume of the FP phase is smaller than that of the $N_{2/3}$FP phase, FP is expected to be in tension, and $N_{2/3}$FP is expected to be in compression during sodiation as well as during desodiation. This mechanical consideration already suggests that the phase transformation in sodiation is alleviated compared with desodiation, an effect that is even discernible in the stress measurements performed at the electrode level.

4. Conclusion

A change in the size of the insertion ion can lead to an enormous change in the electrochemistry of an electrode. Despite the chemical similarity of Li^+ and Na^+, a vastly different electrochemical and mechanical behavior of the FP electrode was found: Different phases form, different kinetics result, and a directional dependence of the electrochemical reaction arises. The substrate curvature method provided data that are complementary to electrochemical measurements and, for example, prove useful in revealing the reaction asymmetry.

Operando substrate curvature measurements on the same FP electrode allowed for a direct comparison between the insertion ions lithium and sodium. The test cell was cycled to about 100 cycles, and for both insertion ions, a high degree of reversibility (coulombic efficiency) was observed. Surprisingly, the mechanical stresses at the electrode level during sodium insertion in FP were about one order of magnitude higher than the stresses that evolve during lithium insertion. This increase of the mechanical stress is roughly four times higher than what can be expected from the expansion of the crystal structure. The unexpectedly high stress levels of the electrode show that mean stresses in composite electrodes cannot be easily predicted by comparing the structure parameters of the constituents.

Morphological changes in the composite electrode were characterized by SEM and show significant changes during sodiation and desodiation. Particles exhibit anisotropic volume changes in agreement with the anisotropic expansion of the crystal lattice during sodiation. Cracks are evolved in the larger particles, and the composite electrode as a whole shows significant long range motion when cycling with sodium. The linear mechanical response of the electrode during lithiation and delithiation is attributed to the two-phase coexistence of LFP and FP and the corresponding electrochemical plateau. For NFP, the stress data showed a very strong asymmetry between sodiation and desodiation. This difference between sodiation and desodiation is suggested to be a consequence of an amorphous phase and the directional dependence of its motion. Motion toward sodium-rich regions requires high stresses and can cause large overpotentials, whereas motion in the opposite direction is alleviated and leads to lower mechanical stress as is observed during sodiation.

It may be expected that many future high capacity materials will exhibit a large lattice mismatch between the phases evolving. Most likely for such electrode materials, widened phase boundaries or even amorphous intermediary phases will play an important role. The fact that the mobility of such intermediary disordered phases/regions intrinsically depends on their direction of motion will cause asymmetric reaction pathways, and due to the associated overpotentials, the energy efficiency of such materials can be significantly compromised.

5. Experimental Section

Experiments were performed on both lithium- and sodium-based batteries by cycling insertion electrodes against the respective metal. For the LIB, commercially available electrolyte (Sigma Aldrich) consisting of 1 M $LiPF_6$ in ethylene carbonate (EC) and dimethyl carbonate (DMC) (1:1) was used. For the SIB, 1 M $NaClO_4$ was dissolved in propylene carbonate (PC) and used as the electrolyte. As the electrode material NFP cannot be chemically synthesized, LFP electrodes were delithiated and sodiated to produce NFP. In this way, the same electrode could be switched between lithium and sodium. The active layer of the starting electrode consisted of 80 wt% LFP powder (Süd-Chemie AG), 10 wt% carbon black, and 10 wt% PVDF binder. It was made by adding the solvent NMP to this mixture of materials and single-side casting the resulting slurry onto a 10 μm thick aluminum foil. After drying, the 67 μm thick (10 μm Al + 56 μm active layer) electrode was cut into pieces and mounted into special test cells for the in situ stress measurements and into Swagelok-type cells for standard electrochemical characterization. Swagelok-type cells were also used for the preparation of SEM samples. In the SEM experiments, the same regions of the electrode were compared before and after selected electrochemical treatments (before use, delithiation, first sodiation, first desodiation). To do this, the cell was disassembled, and the electrode was washed and transferred to the SEM under argon. After the microscopy, the cell was reassembled. For this cell, a combination of Whatman and Celgard separators was selected because this combination is relatively compliant and does not lead to many glass fibers on the electrode surface after disassembly. To reduce bending of the current collector during assembly and disassembly, an aluminum foil with a thickness of 50 μm was glued underneath the standard aluminum current collector.

The cells for stress measurements contained an electrode that was glued onto a borosilicate glass cantilever of a thickness around 155 μm with the dimensions of $\approx 5 \times 15$ mm^2. This cantilever was clamped on one side and immersed into electrolyte. The stainless steel test cells contained a window, and through this window, a laser beam enters the cell and is reflected by the cantilever (**Figure 8**).[32,50] The position

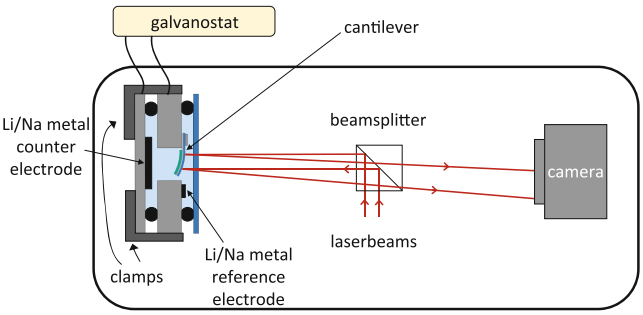

Figure 8. Schematic of the substrate curvature setup. The cell contains the cantilever with the working electrode glued to its left-hand side as well as the metal reference and counter electrodes. Two laser beams are reflected from the cantilever, and their spacing is recorded during cycling. Clamps allow for accurate repositioning of the cell after switching to Na. The electrode shown here is under tension, and the curvature and the resulting angles are exaggerated.

(displacement) of the reflected laser beam linearly depends on the curvature of the cantilever, and therefore, it depends on the mechanical stress in the electrode. As this is a four-layer cantilever containing a thick porous electrode with changing thickness, Stoney's relation is not applicable, and it was not attempted to report quantitative stress values with these experiments. In this work, the curvature/stress data are presented in arbitrary units. As lithium and sodium are compared for the same electrode, a quantitative comparison is still possible by calculating the ratio of the stress amplitudes.

The experiments presented here were performed galvanostatically using a commercial battery cycler (VMP3, Bio-Logic SAS). Lithium cells were cycled between 2.9 and 4.0 V versus Li/Li^+, and the sodium cells were cycled between 2.0 and 4.0 V versus Na/Na^+. To remove lithium from the electrode and to obtain pure FP after a galvanostatic delithiation, a potentiostatic hold at 4 V was carried out until the current dropped below 1/100th of the initial C/10 current. The reference electrode in the curvature cell was dissolved electrochemically to avoid even trace amounts of lithium in the sodium cell. The cells were then opened, the electrode was washed using DMC, and the counter and reference (only in the stress cell) electrodes were replaced by sodium. To be able to make an exact comparison of the mechanical response of lithium and sodium insertion/extraction, it is essential to maintain the same sample position within the substrate curvature setup during all changes of the test cell. Therefore, the electrode itself remained fixed in the same position inside the cell during the transition between lithium and sodium, and repositioning the test cell in the laser setup was facilitated with the help of special clamps (Figure 8).

Acknowledgements

This work was funded by the Deutsche Forschungsgemeinschaft (DFG) within the framework of the research training group SiMET (281041241/GRK2218).

Conflict of Interest

The authors declare no conflict of interest.

Keywords

amorphous phases, iron phosphate, mechanical stress, reaction pathways, sodium ion batteries

Received: October 2, 2020
Revised: November 26, 2020
Published online:

[1] R. D. Shannon, *Acta Crystallogr. A* **1976**, *32*, 751.
[2] D. H. Lee, J. Xu, Y. S. Meng, *Phys. Chem. Chem. Phys.* **2013**, *15*, 3304.
[3] P.-F. Wang, Y. You, Y.-X. Yin, Y.-G. Guo, *J. Mater. Chem. A* **2016**, *4*, 17660.
[4] M. Sathiya, K. Hemalatha, K. Ramesha, J.-M. Tarascon, A. S. Prakash, *Chem. Mater.* **2012**, *24*, 1846.
[5] R. Berthelot, D. Carlier, C. Delmas, *Nat. Mater.* **2011**, *10*, 74.
[6] A. K. Padhi, K. S. Nanjundaswamy, J. B. Goodenough, *J. Electrochem. Soc.* **1997**, *144*, 1188.
[7] L.-X. Yuan, Z.-H. Wang, W.-X. Zhang, X.-L. Hu, J.-T. Chen, Y.-H. Huang, J. B. Goodenough, *Energy Environ. Sci.* **2011**, *4*, 269.
[8] W. Dreyer, J. Jamnik, C. Guhlke, R. Huth, J. Moškon, M. Gaberšček, *Nat. Mater.* **2010**, *9*, 448.
[9] V. Srinivasan, J. Newman, *J. Electrochem. Soc.* **2004**, *151*, A1517.
[10] A. Yamada, H. Koizumi, S. Nishimura, N. Sonoyama, R. Kanno, M. Yonemura, T. Nakamura, Y. Kobayashi, *Nat. Mater.* **2006**, *5*, 357.
[11] G. Kobayashi, S. Nishimura, M.-S. Park, R. Kanno, M. Yashima, T. Ida, A. Yamada, *Adv. Funct. Mater.* **2009**, *19*, 395.
[12] C. Delacourt, P. Poizot, J.-M. Tarascon, C. Masquelier, *Nat. Mater.* **2005**, *4*, 254.
[13] N. Meethong, H.-Y. S. Huang, W. C. Carter, Y.-M. Chiang, *Electrochem. Solid-State Lett.* **2007**, *10*, A134.
[14] P. Gibot, M. Casas-Cabanas, L. Laffont, S. Levasseur, P. Carlach, S. Hamelet, J.-M. Tarascon, C. Masquelier, *Nat. Mater.* **2008**, *7*, 741.
[15] M. Wagemaker, D. P. Singh, W. J. H. Borghols, U. Lafont, L. Haverkate, V. K. Peterson, F. M. Mulder, *J. Am. Chem. Soc.* **2011**, *133*, 10222.
[16] C. Delmas, M. Maccario, L. Croguennec, F. Le Cras, F. Weill, *Nat. Mater.* **2008**, *7*, 665.
[17] J. Wang, Y. K. Chen-Wiegart, J. Wang, *Nat. Commun.* **2014**, *5*, 4570.
[18] A. S. Andersson, B. Kalska, L. Häggström, J. O. Thomas, *Solid State Ionics* **2000**, *130*, 41.
[19] Y. Orikasa, T. Maeda, Y. Koyama, H. Murayama, K. Fukuda, H. Tanida, H. Arai, E. Matsubara, Y. Uchimoto, Z. Ogumi, *Chem. Mater.* **2013**, *25*, 1032.
[20] Y. Orikasa, T. Maeda, Y. Koyama, H. Murayama, K. Fukuda, H. Tanida, H. Arai, E. Matsubara, Y. Uchimoto, Z. Ogumi, *J. Am. Chem. Soc.* **2013**, *135*, 5497.
[21] X.-J. Wang, H.-Y. Chen, X. Yu, L. Wu, K.-W. Nam, J. Bai, H. Li, X. Huang, X.-Q. Yang, *Chem. Commun.* **2011**, *47*, 7170.
[22] D. Wang, X. Wu, Z. Wang, L. Chen, *J. Power Sources* **2005**, *140*, 125.
[23] M. Galceran, D. Saurel, B. Acebedo, V. V. Roddatis, E. Martin, T. Rojo, M. Casas-Cabanas, *Phys. Chem. Chem. Phys.* **2014**, *16*, 8837.
[24] M. Casas-Cabanas, V. V. Roddatis, D. Saurel, P. Kubiak, J. Carretero-González, V. Palomares, P. Serras, T. Rojo, *J. Mater. Chem.* **2012**, *22*, 17421.
[25] B. Özdogru, H. Dykes, S. Padwal, S. Harimkar, Ö. Ö. Çapraz, *Electrochim. Acta* **2020**, *353*, 136594.
[26] P. Moreau, D. Guyomard, J. Gaubicher, F. Boucher, *Chem. Mater.* **2010**, *22*, 4126.
[27] J. Lu, S. C. Chung, S. Nishimura, A. Yamada, *Chem. Mater.* **2013**, *25*, 4557.
[28] K. Xiang, W. Xing, D. B. Ravnsbæk, L. Hong, M. Tang, Z. Li, K. M. Wiaderek, O. J. Borkiewicz, K. W. Chapman, P. J. Chupas, Y.-M. Chiang, *Nano Lett.* **2017**, *17*, 1696.
[29] J. Gaubicher, F. Boucher, P. Moreau, M. Cuisinier, P. Soudan, E. Elkaim, D. Guyomard, *Electrochem. Commun.* **2014**, *38*, 104.
[30] D. Saurel, M. Galceran, M. Reynaud, H. Anne, M. Casas-Cabanas, *Int. J. Energy Res.* **2018**, *42*, 3258.
[31] M. K. Jangid, A. Mukhopadhyay, *J. Mater. Chem. A* **2019**, *7*, 23679.
[32] Z. Choi, D. Kramer, R. Mönig, *J. Power Sources* **2013**, *240*, 245.
[33] T. Zhang, M. Kamlah, *J. Electrochem. Soc.* **2020**, *167*, 020508.
[34] D. Chen, D. Kramer, R. Mönig, *Electrochim. Acta* **2018**, *259*, 939.
[35] A. O. Kondrakov, A. Schmidt, J. Xu, H. Geßwein, R. Mönig, P. Hartmann, H. Sommer, T. Brezesinski, J. Janek, *J. Phys. Chem. C* **2017**, *121*, 3286.
[36] M. Secchiaroli, S. Calcaterra, H. Y. Tran, S. J. Rezvani, F. Nobili, R. Marassi, M. Wohlfahrt-Mehrens, S. Dsoke, *J. Electrochem. Soc.* **2017**, *164*, A672.
[37] J. N. Bridson, S. E. Quinlan, P. R. Tremaine, *Chem. Mater.* **1998**, *10*, 763.
[38] B. L. Ellis, W. R. M. Makahnouk, Y. Makimura, K. Toghill, L. F. Nazar, *Nat. Mater.* **2007**, *6*, 749.
[39] S. P. Ong, V. L. Chevrier, G. Hautier, A. Jain, C. Moore, S. Kim, X. Ma, G. Ceder, *Energy Environ. Sci.* **2011**, *4*, 3680.
[40] W. Ostwald, *Z. Phys. Chem.* **1897**, 289.
[41] T. Threlfall, *Org. Process Res. Dev.* **2003**, *7*, 1017.

[42] S.-Y. Chung, Y.-M. Kim, J.-G. Kim, Y.-J. Kim, *Nat. Phys.* **2009**, *5*, 68.
[43] M. Volmer, A. Weber, *Z. Phys. Chem.* **1926**, *119U*, 277.
[44] M. Avdeev, Z. Mohamed, C. D. Ling, J. Lu, M. Tamaru, A. Yamada, P. Barpanda, *Inorg. Chem.* **2013**, *52*, 8685.
[45] H. J. Fecht, *Nature* **1992**, *356*, 133.
[46] S. Han, L. Zhao, Q. Jiang, J. Lian, *Sci. Rep.* **2012**, *2*, 493.
[47] S. Li, M. S. Sellers, C. Basaran, A. J. Schultz, D. A. Kofke, *Int. J. Mol. Sci.* **2009**, *10*, 2798.
[48] I. A. Blech, C. Herring, *Appl. Phys. Lett.* **1976**, *29*, 131.
[49] M. Meraj, C. Deng, S. Pal, *J. Appl. Phys.* **2018**, *123*, 044306.
[50] A. Al-Obeidi, D. Kramer, R. Mönig, C. V. Thompson, *J. Power Sources* **2016**, *306*, 817.